Production and Mechanical Properties (Strength, Wear, and Fracture Toughness) of Chilled Aluminum—Quartz Castable Particulate Composite

J. Hemanth

(Submitted 15 February 2000; in revised form 12 May 2000)

Structural composite materials offer an excellent opportunity to produce components that achieve weight savings and improved mechanical properties. This paper describes a chilled Al-quartz particulate composite that can be cast using metallic and nonmetallic chill blocks, much like nonreinforced aluminum, using conventional aluminum casting equipments. Unlike other metal matrix composites (MMCs), this material is produced economically by a simple ingot metallurgical process. An overview of the production process is given along with the techniques used for fabricating the chilled composite. The material's mechanical properties, particularly its strength, wear resistance, fracture toughness, and hardness, are discussed in some detail. These properties offer attractive design opportunities for a variety of automotive, aerospace, and structural applications. The composite developed is shown to provide significant weight savings over ferrous metals. The present investigation aims at producing cast aluminum alloy-quartz particulate composites in molds, containing metallic and non metallic chill blocks, by dispersing quartz particles in molten aluminum alloy, above the liquidus temperature, the size of the particles dispersed being between 60 and 100 μm. The dispersoid being added ranges from 3 to 9 wt.% in steps of 3%. The resulting composites cast using chill blocks were tested for their mechanical properties.

Keywords aluminum composites, chill block, composite, fracture toughness, metal matrix, wear

1. Introduction

Reinforcing an aluminum alloy with quartz particles yields a material that displays physical and mechanical properties of both the metal and the quartz. For example, the toughness and formability of aluminum can be combined with some of the strength, hardness, and wear resistance of quartz particles.[1]

It seems probable that metal matrix composites (MMCs) will replace conventional materials in many commercial and industrial applications in the 1990s.[2–5] However, their primary disadvantages for automobile applications are their inferior tensile strength, ductility and poor fracture toughness and fatigue performance, compared to those of the constituent matrix material.[6,7]

2. Literature Review

2.1 Freezing of Aluminum Alloys

It is well known that Al composites freeze over a wide range of temperature and are difficult to feed during solidification.[8] The dispersed porosity caused by the pasty type of solidification of large solidus-liquidus range alloy castings can be effectively reduced by the use of chill blocks. Chill blocks extract heat at a faster rate and promote directional solidification. Therefore, chill blocks are being widely used by the foundrymen in the production of quality castings.[9–15] There have been several investigations[16–24] on the influence of chills on the solidification and soundness of large solidus-liquidus range alloy castings. The present investigation was undertaken because it was apparent from the literature survey that this subject had not been dealt with so far.

2.2 Microporosity in Aluminum Composites

The Al-based composites, widely used in aerospace and automotive industries, are prone to unsoundness in the form of microshrinkage. Microshrinkage or dispersed porosity in the composite can be minimized by the judicious location of chill blocks.[25] J. Redemske, *et al.*,[24] pointed out from their investigation that chilling has an effect on the structure, properties, and soundness of Al alloy castings.

The primary and the most important aspect to be considered in a casting process is the solidification of the casting, because solidification shrinkage contributes substantially to the problems faced during the feeding of castings. In the case of sand molds, the pasty zone poses severe problems; the solution to the problems should aim at establishing a steep temperature gradient during solidification. This can be done by incorporating chill blocks located at predetermined places in the mold. The use of a chill block in the mold seems to be the most popular and the simplest way of establishing a steep temperature gradient in the casting during solidification. When placed judiciously in the mold, the chill block acts as a heat sink through which heat transfer takes place and also establishes steep temperature gradients along the desired direction and in the desired location.[26,27]

J. Hemanth, Department of Mechanical Engineering, Siddaganga Institute of Technology (S.I.T), Tumkur-572 103, Karnataka, India.

Table 1 Chemical composition of the alloy

Elements	Zn	Mg	Si	Cu	Fe	Al
Wt.% composition	3.01	3.00	Traces	Nil	0.001	93.989

2.3 Volumetric Heat Capacity of the Chill Block

The ability of the chill block to extract heat from the molten metal during freezing of the casting is dependent on the size of the chill block and the properties of the chill block material. In other words, the capacity of the chill block to absorb heat from the casting is taken as a measure of its efficiency. The volumetric heat capacity (VHC) of the chill block, which takes into account the volume, specific heat, and density of the chill block material, has been identified as an important factor in evaluating its efficiency.

$$\text{VHC} = V \times C_p \times \rho$$

where

V = volume of the chill block,
C_p = specific heat of the chill block material, and
ρ = density of the chill block material.

It is obvious that a higher value of any one of the factors V, C_p, and or ρ increases the value of VHC, thus enhancing the chilling. On placing a chill block in the mold, heat transfer takes place through the metal-chill interface during solidification.

2.4 Relevance of the Investigation

The Al alloy composites have the potential to replace other costlier material in many significant engineering applications. The requirements concerning safety and reliability are always on the increase, and therefore, the mechanical properties are ever more crucial. From the literature survey, one can easily infer that no investigation has been carried out so forthus far regarding the influence of metallic and non-metallic chill blocks on the mechanical properties of the Al-quartz particulate composite. Because there are presently no published data on Al-quartz chilled composites, the present investigation is intended to fill the void.

3. Experimental Procedure

3.1 Fabrication of Al-Quartz Chilled Composite

Chemical Composition. Chemical composition of the aluminum alloy used as the matrix material is given in Table 1. In this investigation, quartz particles of 3, 6, and 9% by weight were dispersed in the matrix. The chemical composition and properties of quartz particles are as follows: density, 2.9 gm/cc; hardness, 310 BHN; chemical composition, SiO_2 and size distribution of quartz particles, 60 to 100 μm.

Chilled Composite Preparation Procedure. The alloy is introduced into a bottom pouring composite melting furnace. After melting the charge at around 750 °C (heated in an inert atmosphere for 45 minutes at 700 °C), preheated quartz particles at 700 °C are introduced evenly into the molten metal by means of feeding attachments. During this process, the molten metal is well agitated by a mechanical impeller to create vortex motion. The speed of the impeller is maintained at 760 rpm. The process of dispersing the particles is completed within 1 minute. After the complete injection of the dispersoids, the molten metal is again stirred for a few seconds. Later, at 740 °C, it is poured into a mold containing different types of chill blocks.

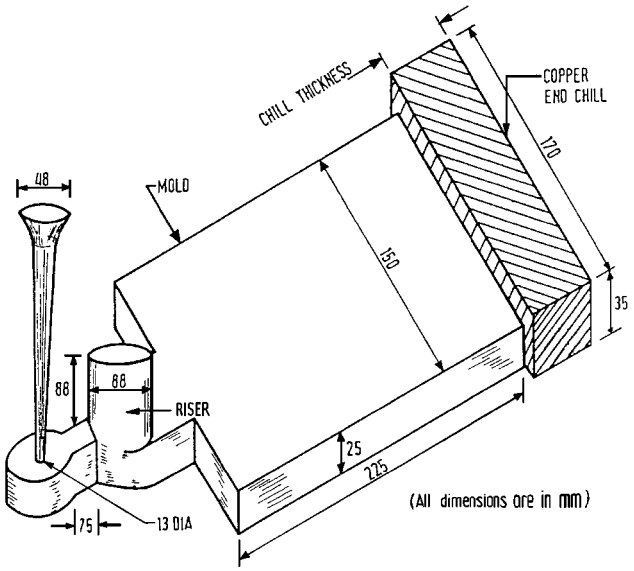

Fig. 1 Experimental setup for production of Al-quartz chilled composite

The molds for the plate type of castings 225 × 150 × 25 mm (American Foundrymen Society (AFS) standard) were prepared using silica sand with 5% bentonite as binder and 5% moisture, and finally, they were dried in an air furnace at a temperature of 80 °C. The dispersoid-treated Al alloy was poured directly into the mold at a pouring temperature of 740 °C, which was cooled from one end by a chill block set in the mold, as shown in Fig. 1.

4. Testing Procedure

4.1 Strength Test Procedure

The specimens for the strength test were taken from various locations in the casting, namely, the chill block end and 75, 150, and 225 mm from the chill block end, the later being at the riser end. Tension tests were performed using an Instron tension testing machine on AFS standard tensometer specimens. Each test result was obtained from an average of at least three samples of the same location. Soundness of the test castings was assessed by determining the percentage porosity and the ultimate tensile strength (UTS).

4.2 Microstructural Examination

Microscopic examination was conducted on all the specimens using a scanning electron microscope (SEM) and an

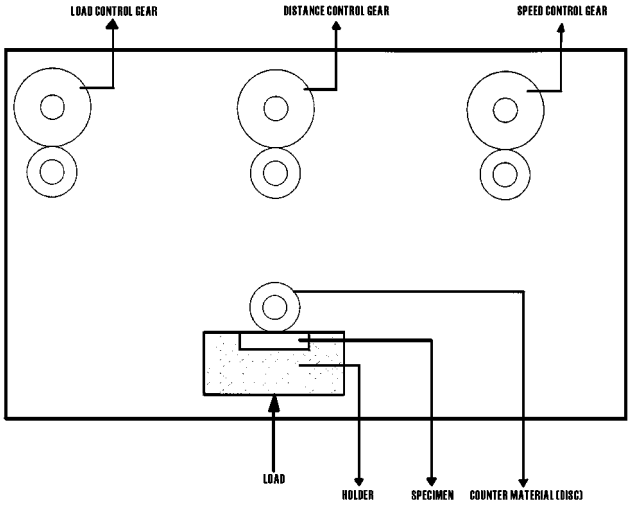

Fig. 2 Diagram of abrasive wear tester

optical microscope. Various etchants were tried, but dilute Kellers etchant proved to be the best and therefore was used.

4.3 Wear and Hardness Test Procedure

Dry wear tests were conducted using the spindle type of wear tester at room temperature. Specimens for the wear and hardness tests were selected at the chill block end of the casting. Figure 2 shows the schematic diagram of the spindle type of wear testing machine. Specimens with dimensions 50 × 20 × 60 mm were machined perpendicular to the direction of the applied pressure. Their surfaces were polished by emery paper (# 600) to achieve uniform surface condition. Oil- quenched SCM 4 were was used as the countermaterial discs. Here, SCM 4 is equivalent to AISI 4140. An electronic balance able to weigh up to 10^{-5} g was used to measure the weight loss of composites. Wear tests were performed under the following conditions: final load, 145 N; sliding distance, 400 m; and various sliding speeds, 0.52, 1.15, 1.98, and 3.64 m/s respectively. After the wear tests, wear surfaces were examined with an SEM. Hardness tests were performed on the wear samples with a Rockwell hardness testing machine (B scale).

4.4 Fracture Toughness Test Procedure

Fracture toughness tests were performed using a closed-loop Instron servo-hydraulic material testing system. The method of testing involves three-point bend testing (in accordance with ASTM E 399 1990 standards) of a machined specimen that has been precracked by fatigue. Fully reversed push-pull, total strain controlled, tension-compression (R = −1) fatigue tests were performed. The tests were performed in a controlled laboratory air environment (temperature, 26 °C; and relative humidity, 56%). An axial 12.5 mm clip-on extensometer was attached to the gauge section of the test specimen to control the total strain. From the load, the stress intensity factor K_{IC} (which is a measure of the fracture toughness of the material) was calculated using equations, which that have been established on the basis of elastic strain analysis. The validity of this method depends on the establishment of a steep crack condition at the tip of the crack in a specimen of adequate size. All the ASTM validity conditions were fulfilled in this experiment.

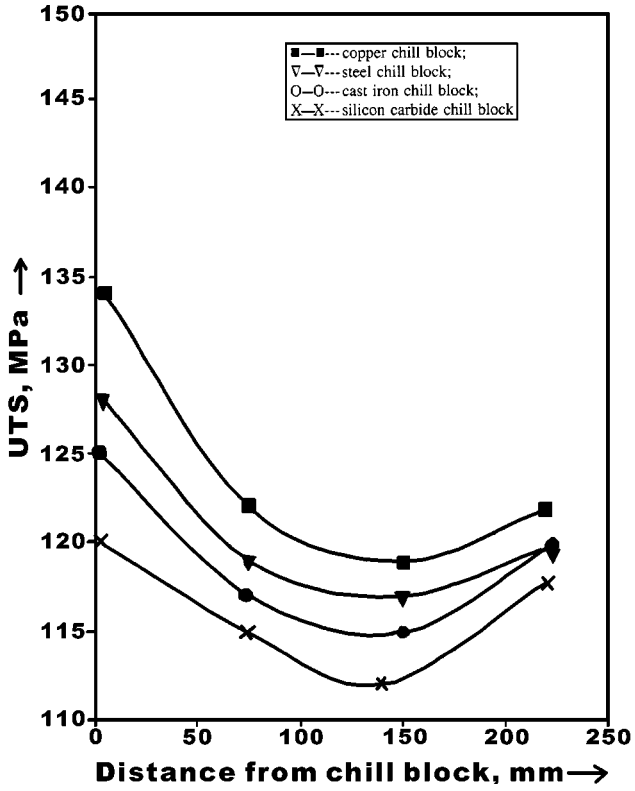

Fig. 3 Plot of UTS vs distance along the length of the casting for different chill block materials (dispersoid content 6 wt.%, cast using copper chill block of 25 mm thickness)

Table 2 UTS of Al-quartz chilled composite for different weight percentages of dispersoid cast using different chill materials (chill block of 25 mm thickness)

	UTS, MPa (near the chill block end)		
Material of chill block	**3 wt.% dispersoid**	**6 wt.% dispersoid**	**9 wt.% dispersoid**
Copper	116	134	129
Steel	114	128	122
Cast iron	102	125	119
Silicon carbide	97	119	112

5. Results and Discussion

5.1 UTS of the Composite

Table 2 shows the UTS for composites near the chill end cast using different types of chill blocks. For all the end chilled plate castings, the UTS of a tensometer specimen was plotted against the distance of the location of the specimen from the chill block end of the casting, as in Fig. 3. Further, it may be observed that the effect of increasing the VHC of the chill

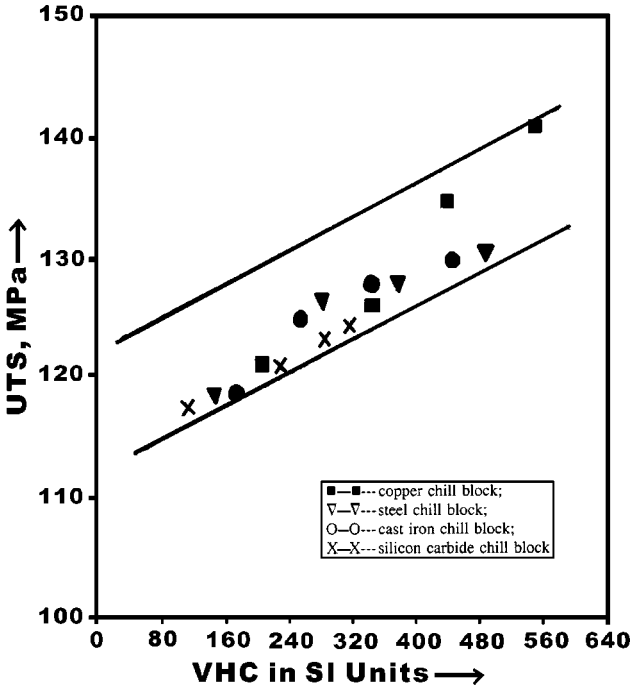

Fig. 4 Plot of UTS vs VHC for different chill block materials (dispersoid 6 wt.%, cast using copper chill block of 25 mm thickness)

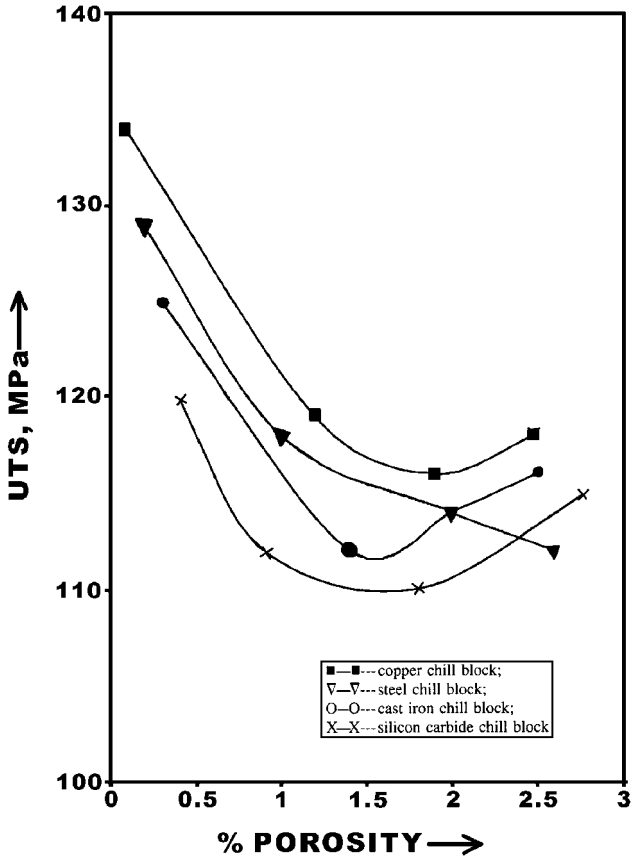

Fig. 5 Plot of UTS vs percentage porosity along the length of the casting (dispersoid 6 wt.%, cast using copper chill block of 25 mm thickness)

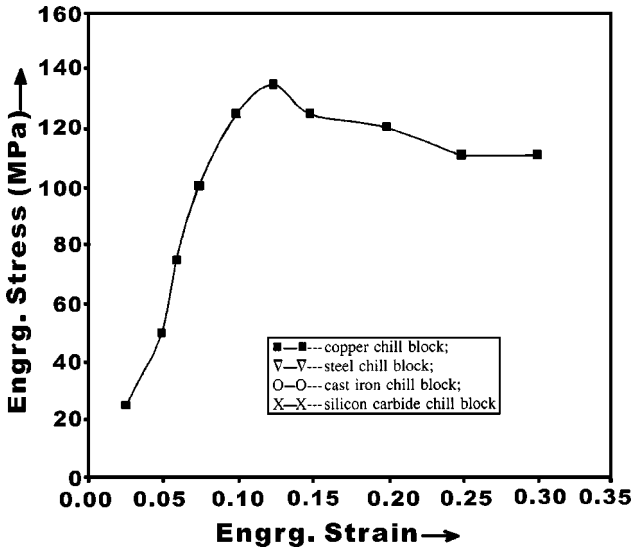

Fig. 6 Engineering stress-strain diagram of the composite cast using copper chill block of 25 mm thickness (dispersoid content 6%)

block (refer to Fig. 4) is to increase the UTS along the length of the casting.

From Fig. 5, it can be seen that the relationship between percentage porosity and UTS is nonlinear. If a tensometer specimen were pore free, its strength would be the strength UTS_{max} of a tensometer specimen machined from the maximum density specimen of the composite.[28–30] And if the tensometer specimen, for the sake of argument, were 100% porous, its mechanical properties would be zero. Hence, the extreme points of the percentage porosity values versus UTS will be (100, 0) and (0, UTS_{max}).

An equation of the form $(\%P/100)^{0.47} + (UTS/UTS_{max})^{0.49} = 1$ was fitted to the experimental data using computer.

Figure 5 indicates that UTS decreases with the increase in percentage porosity. Further, on plotting the data of an earlier investigation by other authors on the effect of end, wedge, and combination of end and wedge chill blocks on the soundness of bar-shaped castings,[31,32] along with the results of the present investigation on plate castings, as shown in Fig. 5, it can be seen that all the points lie within the same band. This implies that, for large solidus-liquidus range alloys, the mechanical properties follow density a pattern.[33] A certain amount of scatter is also observed in the figure. In order to explain this scatter, test specimens were taken along the length of the test castings and were subjected to a systematic macro- and microexamination. Results of the micro- and macroexamination indicate that the shape of the pores and the distribution of the pores in the test specimens are very much dependent on the position of the specimens with respect to the chill block end and the material of the chill block used. Moreover, tensometer specimens occupy a small portion of the cross section of the casting, which may result some at times in a smaller or greater number of pores in the tensometer specimens and hence the scatter. Other researchers[34,35] on Al alloy castings reported a similar relationship. Figure 6 shows the complete stress-strain diagram

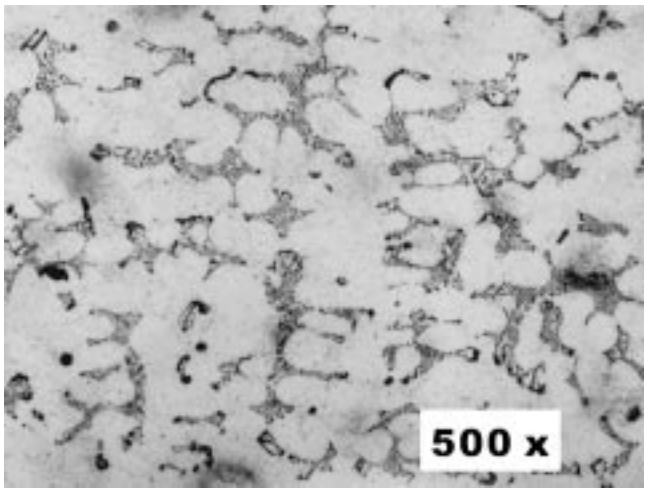

Fig. 7 Microstructure of Al-quartz chilled composite (3 wt.% dispersoid, cast using copper chill block of 25 mm thickness)

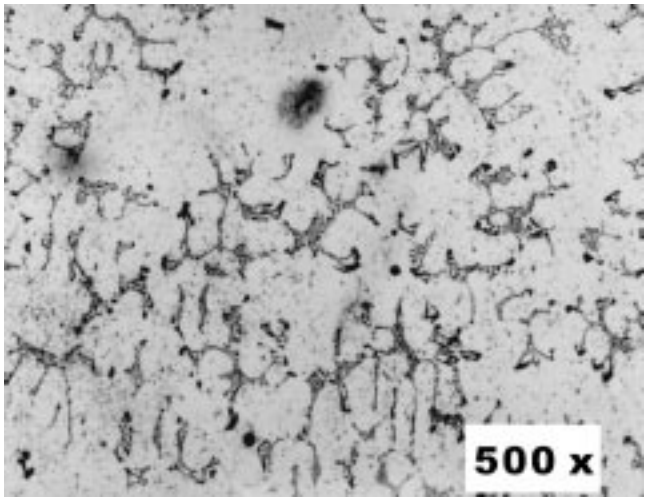

Fig. 8 Microstructure of Al-quartz chilled composite (6 wt.% dispersoid, cast using copper chill block of 25 mm thickness)

of the composite cast using a copper chill block of thickness 25 mm thickness.

In this study, however, the incorporation of quartz as the dispersoid and chilling aimed at improving the wear properties and the mechanical propertiesy such as UTS is also seen.

5.2 Microstructural Observation of the Composite

Microstructural observations of the composite reveal good bonding and good distribution of quartz particles throughout the matrix with none-affective interfacial reaction (refer Fig. 7 and 8). However, tearing is observed at some places. Microstructural observation also indicated that Mg was seen to have migrated to the grain boundaries and particle matrix interfaces; this effect plus and chilling are the possible reasons for good bonding. The most unique feature of chilling the composite in this investigation is the apparent pushing of the solid-liquid interface during solidification and carrying away of the migrated

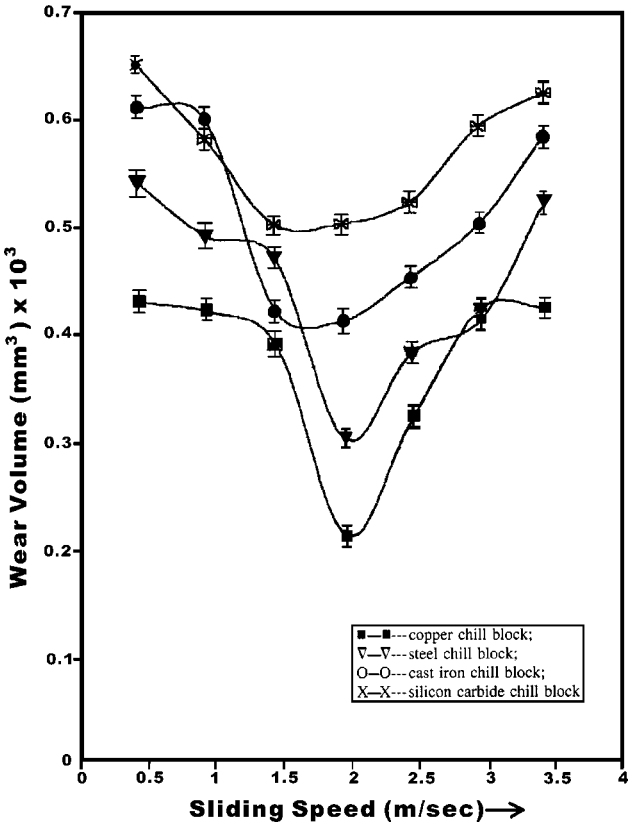

Fig. 9 Effect of sliding speed on wear behavior of Al-quartz chilled composite

Table 3 Hardness of Al-quartz chilled composite for different weight percentages of dispersoid cast using different chill materials (chill block of 25 mm thickness)

	Hardness Rockwell B scale (near chill block end)		
Material of chill block	**3 wt.% dispersoid**	**6 wt.% dispersoid**	**9 wt.% dispersoid**
Copper	87	93	89
Steel	81	86	82
Cast iron	80	83	80
Silicon carbide	72	73	71

alloying elements into the grain boundaries, leaving dispersoids. This may be one of the main reasons for the increase of strength and soundness of the composite developed.

5.3 Wear Behavior

Because the wear resistance of Al alloys is poor, their applications as structural materials and automobile parts are often limited. It has been demonstrated by abrasive wear tests under diverse conditions that the wear resistance of MMCs is improved remarkably by the incorporation of hard particles (quartz). Table 3 shows the hardness of composites near the chill block end cast using different types of materials.

Figure 9 shows the effect of sliding speeds on weight loss

(volume) of Al-quartz composite containing different percentages of quartz particles under a final load of 145 N with a sliding distance of 400 m at various sliding speeds: 0.52, 1.15, 1.98, and 3.64 m/s. On the whole, above the sliding speed of 1.15 m/sec, the wear resistance of the composite improved remarkably. This is due to the bonding of quartz particles with the matrix, which can endure the friction force generated on the wear surface. Thus, friction force plays an important role in wear behavior, especially in abrasive wear. Generally, the higher the friction force generated, the worse the wear resistance.[36]

In the Al-quartz composite, the weight loss of the composite increased continually up to 1.98 m/sec. But, above the sliding speed of 1.98 m/s, the wear loss of the composite increased abruptly. That is, the wear behavior of the composite developed changed along with the sliding speed. It means that the major wear mechanism of the composites developed by chilling is strongly dependent upon the sliding speed. The major wear mechanisms of the chilled composite are abrasive and adhesive wear at sliding speeds up to 1.15 m/s; therefore, an Al-quartz chilled composite is worn by the force of friction generated on the wear surface. Above the sliding speed of 1.15 m/s, the major wear mechanism is shifted to melt wear because of the rise of temperature on the localized wear surface. Consequently, an Al-quartz chilled composite starts to be worn out abruptly. Therefore, the melt wear becomes the major mechanism of wear due to the rise of temperature on the specimen. But the high thermal stability of the composite developed is due to the addition of quartz as dispersoid, and chilling allows only slight deterioration of the wear resistance, compared with unchilled composites with aluminum as the matrix.

5.4 Wear Surface Analysis

The above wear behavior can be explained based on microstructural analysis as follows. Figure 10 represents the overall wear surfaces of the Al-quartz chilled composite containing 6% dispersoid, chilled using copper end chill block at various sliding speeds, 0.52, 1.15, 1.98, and 3.64 m/s, under a final load of 146 N and with a sliding distance of 400 m. Overall wear surfaces of the specimens show a similar trend except at the sliding speed of 1.98 m/s. At a low sliding speed of 0.52 m/s, it was found that abrasive wear was dominant in ploughing and grooving, as indicated by the mark K. That is, the shapes of stripes on the wear surface seem to progressively increase because of abrasive action between the wear specimen and counter material, which might be due, to the high friction force applied on the wear surface.

Compared with Fig. 10(a) and (b), the surface damage in 3% quartz composite is more severe than in those containing 6% quartz. That is, at low sliding speed, the 6% quartz content composite formed grooves by the shearing action of the friction force generated on the wear surface. However, the wear surface of 3% quartz content composites exhibited a number of deep wear grooves. It can thus be considered that, at low sliding speed, the frictional forces of composites are large enough to fracture and pull out the dispersoids from the matrix, and these particles abrade the wear surface of the composite developed.

At an intermediate sliding speed of 1.98 m/s, the damaged section on the wear surface of the composite is shown in Fig. 10(c) and 10(d). Wear debris and distorted surfaces with 3% quartz content composites are more distinguished than in composites with 6% quartz content. From the wear surface, it can be regarded that wear debris and a distorted surface play an important role in wear behavior, *i.e.*, wear progresses by their formation and growth. The formation and growth of this distorted section are illustrated using M and N by an arrow, respectively. The distorted section and debris are formed at the locally fractured area of the matrix alloy. This localized fracture is caused by highly localized friction forces, which have form the non uniform surface of the counter material and defected areas of the wear surface. The growth of the damaged section is advanced by the fracture of the wear surface. Wear surfaces of 3% quartz composite show that abrasive and adhesive wear is the dominant wear mechanism at intermediate sliding speeds. By contrast, the wear surface of 6% quartz composite is completely different from that of the 3 % quartz chilled composite. That is, the wear surface of 6% quartz chilled composites, abrasion of dispersoids, and the matrix is are seldom observed due to the remarkable reduction of friction forces applied to the wear surface. Figure 10(d) illustrates an alumina fiber being pulled out (see shown by the arrow) and being struck on the wear surface.

As the sliding speed increases, adhesive and slip phenomena also appear at the high sliding speed of 3.68 m/s. Here, removed materials can determine adhesive wear and slip phenomena can also be found in the wave patterns of materials. The removal of the material seems to be accelerated by fractures of short alumina fibers and the matrix, which might be due to the high friction force applied on the wear surface. Wear surfaces of 3% quartz copper chilled composite and 6% quartz copper chilled composite at a sliding speed of 3.68 m/sec are shown in Fig. 10(e) and (f), respectively. Localized melted areas owing to the rise of temperature are observed in both the composites. As shown in Fig. 9(e), wear of 3% quartz chilled composite seems to start by localized melting of the surface and to proceed by delaminations from the large plastic deformation of the matrix. In the 6% quartz chilled composite shown in Fig. 10(f), some wear patterns such as wave shape, which might be related to melt and slip indicated by an arrow (P), are often seen. These figures illustrate that the major wear mechanisms at high sliding speeds are melt and slip wear of the matrix due to the rise of temperature, and less severe damage on the wear surface is also seen compared with copper chilled composites.

5.5 Fracture Toughness

The manner in which stress response varies with cycles and plastic-strain amplitude is an important feature of the low-cycle fatigue process. The cyclic stress required for pre-cracking the specimen, providing provides useful information pertaining to the mechanical stability of the intrinsic microstructural features during reverse plastic straining, and the ability of the material to distribute the plastic strain over the entire volume, are the two key factors governing the cyclic response of a material.[37]

The experimental results of the fracture toughness tests done on castings chilled using 25 mm thick metallic chill blocks are shown in Table 4. Comparing the results, it can be seen that changing the type of chill block seems to have an effect on the fracture toughness of the material. This implies that increasing

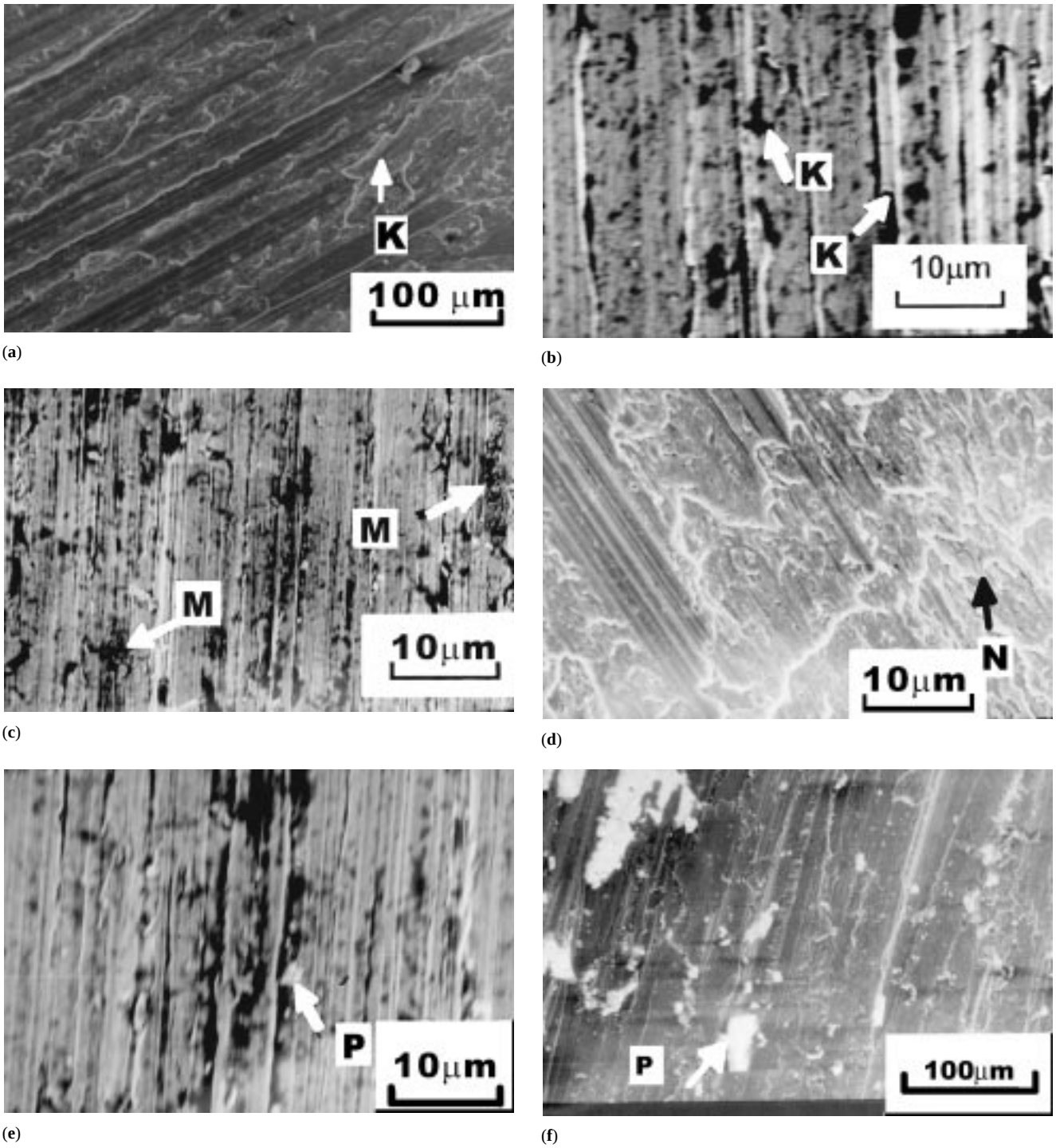

Fig. 10 Wear surfaces of Al-quartz chilled composite at various sliding speeds (cast using copper chill block of 25 mm thickness). (**a**) and (**b**): Sliding speed: 0.52 m/s for composites containing 3 and 6 wt.% dispersoid. (**c**) and (**d**) Sliding speed: 1.98 m/s for composites containing 3 and 6 wt.% dispersoid. (**e**) and (**f**) Sliding speed: 3.68 m/s for composites containing 3 and 6 wt.% dispersoid

the rate of chilling by increasing the volumetric heat capacity of the chill block tends to result in an increase in the fracture toughness of the material. Of more significant effect is the quartz content of the specimen. It can be seen that, if all other factors are kept constant, castings chilled using copper block invariably haves the highest fracture toughness followed by steel, cast iron, and silicon carbide chilled composites in that order. Further, it is observed that, at quartz contents beyond 6 wt.%, the values register a decrease in fracture toughness. It is also observed that the farther away from the chill the specimen is taken, the lower is the fracture toughness. This could be because the farther away from the chill the specimen is, the

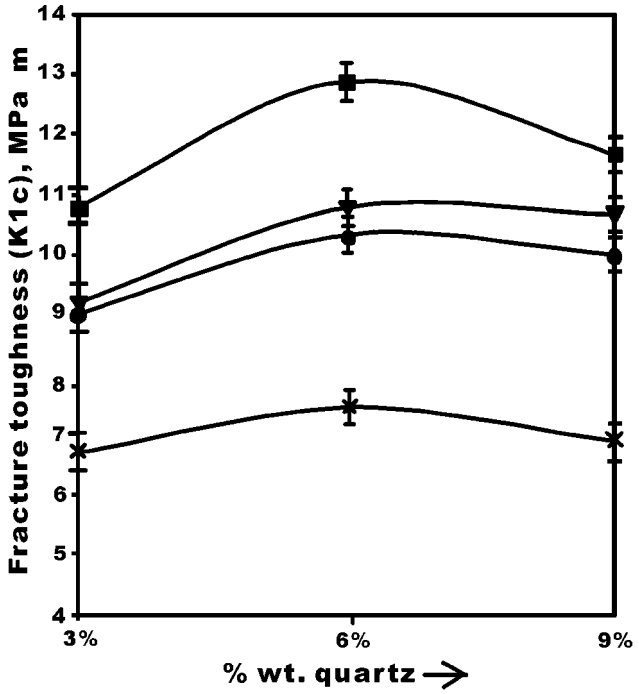

Fig. 11 Effect of fracture toughness on quartz content (cast using chill blocks of different materials)

Table 4 Fracture toughness of Al-quartz chilled composite for different weight percentages of dispersoid cast using different chill materials (chill block of 25 mm thickness)

	Fracture toughness (K_{IC}), MPa$\sqrt{m}$ (near the chill block end)		
Material of chill block	**3 wt.% dispersoid**	**6 wt.% dispersoid**	**9 wt.% dispersoid**
Copper	11	13	12
Steel	9	11	11
Cast iron	9	10	9
Silicon carbide	6	7	7

lower is the rate of chilling. This agrees with the deductions made earlier that increasing the rate of chilling tends to result in an increase in the fracture toughness of the material.[38]

The fracture toughness of the composite chilled using different types of chills versus the quartz content is shown in Fig. 11. The presence of quartz in the chilled composite has a pronounced effect on the fracture toughness. The mechanisms, which control the variation of fracture toughness of chilled Al-quartz composites, are dependent upon both microstructure and strain range. The possible micromechanisms controlling the fracture behavior during cyclic loading are ascribed to the following synergistic influences:

- load transfer between the soft aluminum matrix and the hard and brittle quartz particle reinforcement;
- a pre-existing high dislocation density in the aluminum matrix caused by the presence of the hard, brittle quartz particles;
- hardening arising from constrained plastic flow and triaxibility in the aluminum matrix due to the presence of the brittle quartz reinforcements (as a direct result of the particles resisting the plastic flow of the matrix, especially in chilled composites, an average internal stress or back stress is created);
- dislocations arising from competing influences of back stresses in the plastically deforming composite matrix and due to plastic relaxation by the formation of dislocation loops around the hard quartz particles; and
- residual stresses generated in the matrix and dislocations arising due to the mismatch in thermal expansion coefficients between the components of the composite, *i.e.*, the soft aluminum matrix and the hard reinforcing quartz.

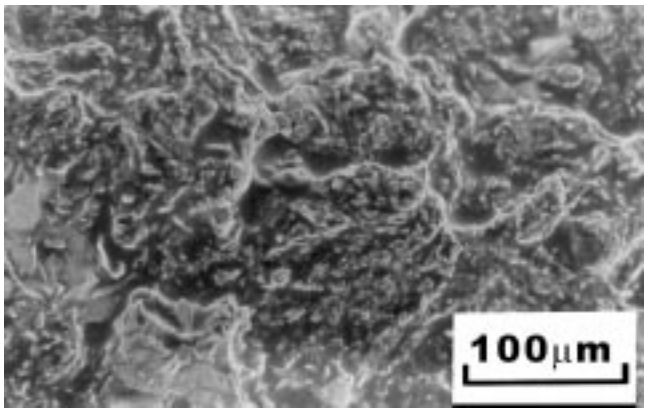

Fig. 12 Fractograph of Al-quartz chilled composite (3 wt.% dispersoid, cast using copper chill block of 25 mm thickness)

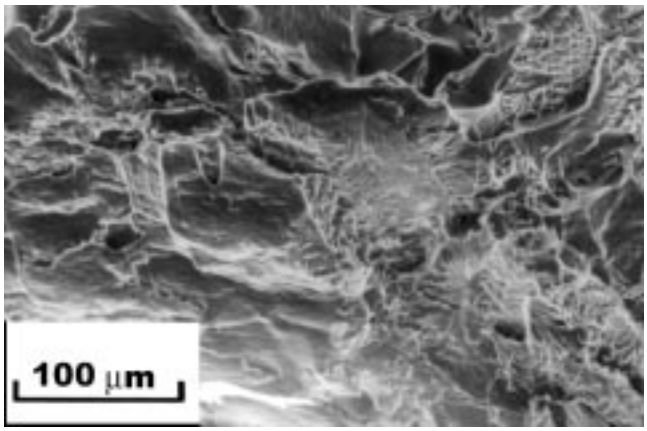

Fig. 13 Fractograph of Al-quartz chilled composite (3 wt.% dispersoid, cast using copper chill block of 20 mm thickness)

Examination of the fracture surface features (Fig. 12 to 15) in the SEM of the fractured fatigue specimens specimens in the SEM was at performed at low magnification to identify the fatigue and final fracture regions, and at higher magnification in the fatigue region to identify regions of micro-crack initiation

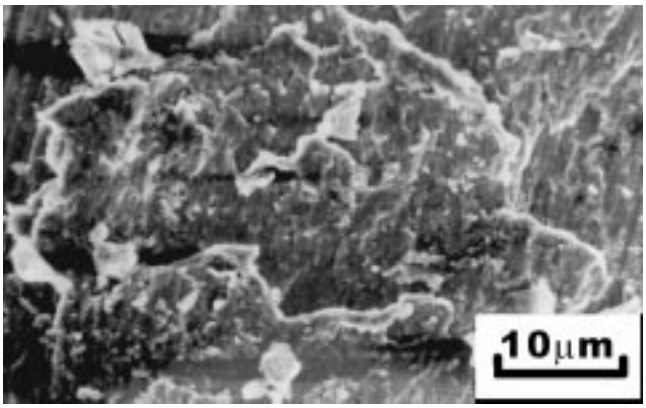

Fig. 14 Fractograph of Al-quartz chilled composite (3 wt.% dispersoid, cast using steel chill block of 25 mm thickness)

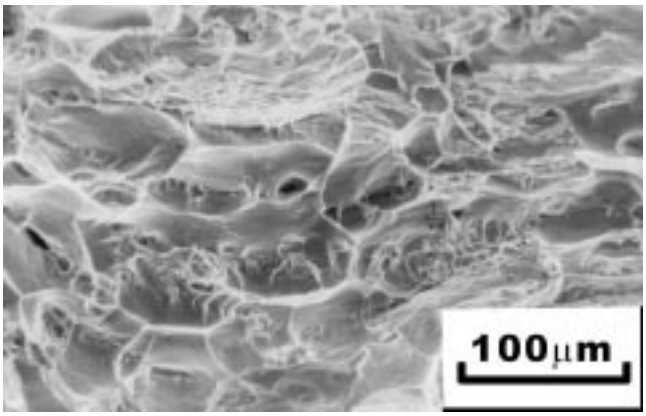

Fig. 15 Fractograph of Al-quartz chilled composite (3 wt.% dispersoid, cast using steel chill block of 20 mm thickness)

and early crack growth, and the over-loaded region to identify the fine scale fracture features. Fracture surfaces revealed different topographies for the composites containing different weight percentages of quartz particles cast using different types of chill blocks.

Cyclic fracture of the chilled cast microstructure on a macroscopic and microscopic scale, exhibited ductile fracture with isolated micro-cracks in the matrix (Fig. 12 and 13). Observations revealed large areas of the fracture surface to be covered with a bimodal distribution of dimples, indicative of ductile rupture (Fig. 14 and 15). A dimple is a half void. The void forms at the coarse second-phase particles, namely, the iron and silicon intermetallic contained in the aluminum matrix. However, growth of the void is limited by by the competing and synergistic influence of the reinforcing quartz particles and the cyclic ductility of the composite microstructure.

Conversely, cyclic fracture of the as-cast microstructure (unchilled) on a microscopic scale, exhibited limited ductility with fracture essentially normal to the stress axis;, low magnification observations revealed the fracture to be brittle with cracking in the direction of the major stress axis.

During cyclic deformation, it seems possible that the mismatch that exists between the brittle reinforcing particle and the ductile matrix favors concentration of stress at and near the particle/matrix interface, causing the matrix in the immediate vicinity to fail permanently or the particle to separate from the matrix. Thus, the fracture behavior of the chilled aluminum-quartz composite records well with the improved fracture toughness over the as-cast (un-chilled) composite.

6. Conclusions

In the present investigation, of all the chill blocks, the copper chill block was found to be the most effective because of its high VHC. A dispersoid content up to 6 wt.% was found to increase the mechanical properties, and therefore, it is considered as the optimum limit. Hence, the present discussion is mainly based on chilled Al-quartz composite with 6 wt.% dispersoid chilled using a copper chill block. Therefore, the introduction of a chilled Al-quartz composite material represents a revolutionary development in the field of MMCs technology for the following reasons.

- For the first time, the engineering benefits of Al-quartz based composites can now be realized in the form of chilled castings.
- The new composite developed is very inexpensive compared with MMC materials manufactured by traditional methods.
- Chilled Al-quartz composites were successfully fabricated by employing chill blocks. From their microstructure, it was found that there is uniform distribution of the dispersoid, and good bonding between the matrix and the dispersoid was achieved.
- The UTS values of the chilled composites were increased by increasing the addition of dispersoids up to 6 wt.%. Copper end chill block was found to be more effective than compared with the other types of chill blocks.
- Wear resistance of copper chilled composites was remarkably improved by adding quartz particles. The effects of amounts of quartz contents up to 3% can be ignored until the sliding speed of 0.52 m/s. Specifically, at the intermediate sliding speed of 1.15 and 1.98 m/s, the wear resistance of copper chilled composite containing 6% quartz was found to be better than that of the rest of the composites chilled using other types of chill blocks.
- From the SEM structure studies, wear surfaces of 6% quartz copper chilled composite at low sliding speed showed slighter groove formations than those of the matrix alloy. This abrasive wear was seen in photomicrographs analysis due to the frictional forces, which were large enough to fracture and pull out the dispersoids from the matrix. At intermediate sliding speeds, damaged sections in the wear surfaces of the composites were seldom observed. At high sliding speed, localized melt and slip and large plastic deformations due to the high frictional heat are the dominant factors contributing to the removal of MMCs.
- The fracture behavior of the as-cast (unchilled) composite revealed brittle failure with separation of the quartz particles from the matrix. The existence of weak constraints at

the quartz/matrix interface, coupled with the stress concentration effects, causes the particles to easily crack and separate from the matrix, whereas fracture behavior of the chilled composite shows ductile rupture with isolated microcracks and a bimodal distribution of dimples on the fracture surface.

References

1. Joel Hemanth: *J. Alloys and Compounds,* 2000, vol. 296, p. 193.
2. S.Q. Wu, H.Z. Wang, and S.C. Tjong: *Composite Sci. Technol,* 1996, vol. 56, p. 1261.
3. S.C. Tjong, S.Q. Wu, and H.C. Liao: *Composite Sci. Technol.,* 1997, vol. 57, p. 1551.
4. W.C. Harrigan: Trans AIME, Warrendale, PA, 1983, vol. 27, p. 169.
5. C.M. Friend: *J. Mater. Sci.,* 1987, vol. 22, p. 3005.
6. C.R. Crowe, R.A. Gray, and D.F. Haryson: TMS-AIME, Warrendale, PA, USA, 1985, vol. 32, p. 843.
7. J.J. Lewandowski, C. Liu, and W.H. Hunt: TMS-AIME, Warrendale, PA, 1985, vol. 33, p. 483.
8. G.P. Reddy and P.K. Pal: *Br. Foundryman,* 1976, vol. 69, p. 265.
9. Joel Hemanth and K.H.W. Seah: *SME Year Book,* Tu Myint, SME, ed., Singapore Chapter - 219, EM94-154, 1994, p. 31.
10. Joel Hemanth: *J. Mater. Design,* 2000, vol. 21, p. 01.
11. Joel Hemanth and K.H.W. Seah: *J. Mater. Science,* 1995, vol. 30, p. 4986.
12. Joel Hemanth and K.H.W. Seah: *J. Wear,* 1996, vol. 192, p. 134.
13. Joel Hemanth and K.H.W. Seah: *J. Mater. Design,* 1995, vol. 16, p. 175.
14. Joel Hemanth and K.H.W. Seah: *J. Mater. Science,* 1998, vol. 33, p. 23.
15. Joel Hemanth: *J. Mater. Design,* 1998, vol. 19, p. 269.
16. W.D. Walther, C.M. Adams, and H.F. Taylor: *Trans. AFS,* 1954, vol. 62, p. 219.
17. R.W. Ruddle: *J. Inst. Mater., London,* 1950, vol. 77, p. 37.
18. R.A. Flinn and H.G. Kunsmann: *Trans. AFS,* 1959, vol. 67, p. 385.
19. A. Couture and Meier: *Trans. AFS,* 1966, vol. 74, p. 164.
20. M.V. Chamberlin and J.G. MeZoff: *Trans. AFS,* 1946, vol. 54, p. 648.
21. S. Seshan and M.R. Seshadri: *Br. Foundryman,* 1968, vol. 61, p. 339.
22. J.T. Berry: *Trans. AFS,* 1970, vol. 78, p. 421.
23. K.V. Prabhakar and K.S.S. Murthy: *Trans. AFS,* 1979, vol. 87, p. 377.
24. J. Redemske, G. Prokuda, and M.J. Weins: *Trans. AFS,* 1977, vol. 85, p. 609.
25. K. Radhakrishna and S. Seshan: *Trans. AFS,* 1981, vol. 89, p. 158.
26. D.J. Towle and C.M. Friend: *J. Scripta Metall.,* 1992, vol. 26, p. 437.
27. Joel Hemanth and K.V.S. Rao: *JMEP,* 1999, vol. 8, p. 45.
28. M. Taya and R.J. Arsenault: *Corrosion Sc.*, Pergamon Press, Elmsford, NY, 1989, vol. 32, p. 281.
29. K.S.S. Murthy, M.R. Seshadri, and S. Seshan: *Br. Foundryman,* 1964, vol. 52, p. 451.
30. K.S.S. Murthy, A. Ramachandra, and M.R. Seshadri: *Metalen,* 1964, vol. 19, p. 367.
31. W.R. Roberts and V. Kondic: *Modern Castings,* 1962, vol. 42(4), p. 67.
32. K.S.S. Murthy and S. Mahadevan: *Trans. AFS,* 1965, vol. 73, p. 502.
33. K.S.S. Murthy and S. Seshan: *34th Int. Foundry Congr.,* Paris, 1967.
34. S. Jacob and M. Drouzy: *Foundrie,* 1970, Dec., p. 395.
35. S. Seshan, M.R. Seshadri, and K.S.S. Murthy: *Br. Foundryman,* 1968, vol. 61, p. 3.
36. S.V. Prasad and K.R. Mecklenburg: *J. Wear,* 1993, vol. 162, p. 47.
37. E.A. Starke and G. Lutjering: *J. of Mater. Eng. and Performance,* ASM International., Metals Park, OH, 1979, vol. 14, p. 205.
38. Joel Hemanth: *J. Mater. Sci. Technol.,* 1999, vol. 15, p. 201.